Implicit solution of the 4-field extended-magnetohydrodynamic equations using high-order high-continuity finite elements

S. C. Jardin and J. A. Breslau

Plasma Physics Laboratory, Princeton University, P.O. Box 451, Princeton, NJ 08543

November 13, 2004

Abstract

Here we describe a technique for solving the 4-field extended-magnetohydrodynamic (MHD) equations in 2 dimensions. The introduction of triangular high-order finite elements with C^1 continuity leads to a compact representation compatible with direct inversion of the associated sparse matrices. The split semi-implicit method is introduced and used to integrate the equations in time, yielding unconditional stability for arbitrary time step. The method is applied to the cylindrical tilt mode problem with the result that a non-zero value of the collisionless ion skin depth will increase the growth rate of that mode. The effect of this parameter on the reconnection rate and geometry of a Harris equilibrium and on the Taylor reconnection problem is also demonstrated. This method forms the basis for a generalization to a full extended-MHD description of the plasma with 6, 8, or more scalar fields.

PACS category: 52.30 Ex
Keywords: Magnetohydrodynamics, two-fluid, numerical methods, finite elements

Tel.: +1-609-243-2635
E-mail addresses: jardin@pppl.gov, jardin@princeton.edu (S.C. Jardin)

I. Introduction

It has been recognized for some time that it is necessary to go beyond the simple "resistive MHD" description of the plasma in order to get the correct quantitative results for the growth and saturation of global dissipative modes in a fusion device. The inclusion of a more complete "generalized Ohms law" and the off-diagonal terms in the ion pressure tensor introduce whistler waves, kinetic Alfvén waves, and gyro-viscous waves, all of which are dispersive and require special numerical treatment. We describe a numerical approach to solving these extended-MHD equations using a compact representation that is specifically designed to yield efficient, high-order-of-accuracy implicit solutions of a general formulation of the extended-MHD equations. The representation is based on a triangular finite element with fifth order accuracy that is constructed to have continuous derivatives across element boundaries. The Galerkin technique allows this element to be applied to systems of equations containing spatial derivative operators of up to 4th order. The final set of discrete block matrix equations is solved using a parallel sparse direct solver.

For the general formulation, the magnetic and velocity fields are decomposed without loss of generality in a potential, stream function form as in [1]. Formulating the problem in these variables allows two non-trivial subsets of equations that can be studied before embarking on the full set of equations. The 2-variable system described in [2] is the well known 2-field “reduced MHD” equations consisting of a single flux function for the magnetic field and a single stream function for the velocity. The present paper describes the method applied to a more complex subsystem: the 4-field reduced MHD equations, also known as the reduced two-fluid MHD equations. This set of equations contains both MHD behavior associated with the shear Alfvén wave and the essential features of the whistler and kinetic Alfvén wave physics. Variations of these equations have been extensively studied in the literature [3-5].

We present the 4-field equations in Sec. II, and then describe the split semi-implicit method for their solution in Sec. III and the numerical stability of this method in Sec. IV. Sections V, VI, and VII present applications of this method to three model problems: presenting new results on the effect of the collisionless ion skin depth on the growth rate of the tilt mode in Sec. IV and confirming the importance of this term on reconnection rates in Secs. VI and VII. The paper is summarized with discussion in Sec. VIII.

II. The Equations

The reduced two-dimensional (*x*,*y*) two-fluid MHD equations in the limit of zero electron mass can be written [3]

$$\frac{\partial}{\partial t}\nabla^2\phi = \left[\phi,\nabla^2\phi\right] + \left[\nabla^2\psi,\psi\right] + \mu\nabla^4\phi \qquad (1a)$$

$$\frac{\partial V_z}{\partial t} = \left[\phi,V_z\right] + \left[I,\psi\right] + \mu\nabla^2 V_z - \mu h\nabla^4 V_z \qquad (1b)$$

$$\frac{\partial\psi}{\partial t} = \left[\phi,\psi\right] + d_i\left[\psi,I\right] + \eta\nabla^2\psi - \nu\nabla^4\psi \qquad (1c)$$

$$\frac{\partial I}{\partial t} = [\phi, I] + d_i\left[\nabla^2\psi,\psi\right] + \left[V_z,\psi\right] + \eta\nabla^2 I - \nu\nabla^4 I \tag{1d}$$

where we have utilized the Poisson bracket notation:

$$[a,b] \equiv \nabla a \times \nabla b \cdot \hat{z}$$

Here, ϕ is the in-plane velocity stream function, V_z is the *z*-component of the velocity, ψ is the magnetic flux function, and *I* is the *z*-component of the magnetic field. Thus, the magnetic field and (incompressible) fluid velocity are represented as: $\vec{B} = \nabla\psi \times \hat{z} + I\hat{z}$; $\vec{V} = \nabla\phi \times \hat{z} + V_z\hat{z}$. It is shown in [3] that Eqs. (1a-d) are valid in the low guide-field limit in which whistler waves are the dominant 2-fluid effect, but that a very similar set of equations is valid in the high guide-field limit in which the kinetic Alfvén wave is prominent. Thus, we take the Eqs. (1) to be typical of the extended MHD equations in 2D.

The fluid viscosity, electrical resistivity, hyper-resistivity (or electron viscosity) and collisionless ion skin depth are given by μ, η, ν, and d_i. (The parameter *h* is a hyper-viscosity coefficient added to damp spurious oscillations that might otherwise develop.) Terms involving the electron mass have been neglected. The 2-field reduced MHD system studied in [1] are just Equations (1a) and (1c) with the parameter d_i set to zero.

The equations (1) have the energy integral (in the absence of sources):

$$\tfrac{1}{2}\frac{\partial}{\partial t}\iint\left\{|\nabla\phi|^2 + V_z^{\,2} + |\nabla\psi|^2 + I^2\right\}dA = -\iint\left\{\begin{matrix}\mu\left|\nabla^2\phi\right|^2 + \mu\left|\nabla V_z\right|^2 + \eta\left|\nabla^2\psi\right|^2 + \eta\left|\nabla I\right|^2 \\ +\mu h\left|\nabla^2 V_z\right|^2 + \nu\left|\nabla(\nabla^2\psi)\right|^2 + \nu\left|\nabla^2 I\right|^2\end{matrix}\right\}dA \tag{2}$$
$$+\oint d\ell\,\hat{n}\bullet\nabla\psi\nabla^2\psi$$

To derive (2), we have assumed the perturbed variables obey the boundary conditions:
$\tilde{\phi} = \mu\hat{n}\bullet\nabla\tilde{\phi} = \tilde{V}_z = \mu h_1\hat{n}\bullet\nabla\tilde{V}_z = \tilde{\psi} = \nu\nabla^2\tilde{\psi} = \tilde{I} = \nu\hat{n}\bullet\nabla\tilde{I} = 0$

III. The Numerical Method:

To derive the implicit system, we Taylor expand the RHS of Eq. (1) in time to center the spatial derivatives at the advanced time: $t^{n+\theta} \equiv t^n + \theta\delta t$, keeping only the terms through first order in the time step δt. This gives

$$\begin{aligned}\nabla^2\dot{\phi} = &\left[\phi,\nabla^2\phi\right] + \theta\delta t\left[\dot{\phi},\nabla^2\phi\right] + \theta\delta t\left[\phi,\nabla^2\dot{\phi}\right] + \left[\nabla^2\psi,\psi\right] \\ &+ \theta\delta t\left[\nabla^2\dot{\psi},\psi\right] + \theta\delta t\left[\nabla^2\psi,\dot{\psi}\right] + \mu\nabla^4\phi + \theta\delta t\mu\nabla^4\dot{\phi}\end{aligned} \tag{3a}$$

$$\begin{aligned}\dot{V}_z = &\left[\phi,V_z\right] + \theta\delta t\left[\dot{\phi},V_z\right] + \theta\delta t\left[\phi,\dot{V}_z\right] + \left[I,\psi\right] + \theta\delta t\left[\dot{I},\psi\right] + \theta\delta t\left[I,\dot{\psi}\right] \\ &+ \mu\nabla^2 V_z + \mu\theta\delta t\nabla^2\dot{V}_z - \mu h\nabla^4 V_z - \mu h\theta\delta t\nabla^4\dot{V}_z\end{aligned} \tag{3b}$$

$$\dot{\psi} = [\phi,\psi] + \theta\delta t\left[\dot{\phi},\psi\right] + \theta\delta t[\phi,\dot{\psi}] + d_i[\psi,I] + d_i\theta\delta t[\dot{\psi},I] + d_i\theta\delta t\left[\psi,\dot{I}\right] \\ + \eta\nabla^2\psi + \eta\theta\delta t\nabla^2\dot{\psi} - \nu\nabla^4\psi - \nu\theta\delta t\nabla^4\dot{\psi} \tag{3c}$$

$$\dot{I} = [\phi,I] + \theta\delta t\left[\dot{\phi},I\right] + \theta\delta t\left[\phi,\dot{I}\right] + d_i\left[\nabla^2\psi,\psi\right] + d_i\theta\delta t\left[\nabla^2\dot{\psi},\psi\right] + d_i\theta\delta t\left[\nabla^2\psi,\dot{\psi}\right] \\ + [V_z,\psi] + \theta\delta t\left[\dot{V}_z,\psi\right] + \theta\delta t[V_z,\dot{\psi}] + \eta\nabla^2 I + \eta\theta\delta t\nabla^2\dot{I} - \nu\nabla^4 I - \nu\theta\delta t\nabla^4\dot{I} \tag{3d}$$

The *split semi-implicit* method consists of using Eqs. (3c) and (3d) , but with the field time derivatives $\dot{\psi}$ and $\dot{I}$ on the right of the equal sign set to zero and ignoring (small) dissipative terms, to eliminate time derivatives $\dot{\psi}$ and $\dot{I}$ from Eqs. (3a) and (3b). This has the effect of isolating the linearized Alfven wave characteristics in those two equations. Thus, the modified velocity equations become:

$$\begin{aligned}\nabla^2\dot{\phi} &= \left[\phi,\nabla^2\phi\right] + \left[\nabla^2\psi,\psi\right] + \mu\nabla^4\phi + \\ &+ \theta\delta t\begin{Bmatrix}\left[\nabla^2\left([\phi,\psi]+d_i[\psi,I]\right),\psi\right] + \left[\nabla^2\psi,\left([\phi,\psi]+d_i[\psi,I]\right)\right] \\ +\left[\dot{\phi},\nabla^2\phi\right] + \left[\phi,\nabla^2\dot{\phi}\right] + \mu\nabla^4\dot{\phi}\end{Bmatrix} \\ &+ (\theta\delta t)^2\left\{\left[\nabla^2\left[\dot{\phi},\psi\right],\psi\right] + \left[\nabla^2\psi,\left[\dot{\phi},\psi\right]\right]\right\}\end{aligned} \tag{3a$'$}$$

and

$$\begin{aligned}\dot{V}_z &= [\phi,V_z] + [I,\psi] + \mu\nabla^2 V_z - \mu h\nabla^4 V_z \\ &+ \theta\delta t\begin{Bmatrix}\left[\left([\phi,I] + d_i\left[\nabla^2\psi,\psi\right] + [V_z,\psi]\right),\psi\right] \\ +\left[I,\left([\phi,\psi]+d_i[\psi,I]\right)\right] + \left[\dot{\phi},V_z\right] + \left[\phi,\dot{V}_z\right] \\ +\mu\nabla^2\dot{V}_z - \mu h\nabla^4\dot{V}_z\end{Bmatrix} \\ &+ (\theta\delta t)^2\left\{\left[\left(\left[\dot{\phi},I\right] + \left[\dot{V}_z,\psi\right]\right),\psi\right] + \left[I,\left[\dot{\phi},\psi\right]\right]\right\}\end{aligned} \tag{3b$'$}$$

The system (3a)′ , (3b)′ , (3c) and (3d) is solved each time step as two pairs of equations, with Eqs. (3a)′ and (3b)′ being solved first to obtain the velocity time derivatives $\dot{\phi}$ and $\dot{V}_z$, and these being substituted into Eqs. (3c) and (3d), which are then solved to obtain the field time derivatives $\dot{\psi}$ and $\dot{I}$.

The motivation is to form two compact systems that can be efficiently solved each time step using elementary matrix methods. The Courant time step restriction associated with the Alfvén waves is eliminated by the implicit simultaneous solution of (3a)′ and (3b)′ . Since Eqs. (3c) and (3d) contain the mechanism for the whistler waves, at least in the electron MHD (EMD) model [6], these can next be solved implicitly to remove the severe time step restriction associated with the dispersive whistler waves.

A similar technique, but applied to the Alfvén wave only, has been called the "differential approximation" in [7] and [8]. The present treatment differs from those in the time-centering of the variables and in the retention of terms linear in δt in the modified equations (3a)′ and (3b)′. However the major difference between this and previous work is in the extension of this technique to the whistler wave through equations (3c) and (3d). The numerical stability of this system is discussed in Sec. IV.

To obtain the discrete matrices, we first finite difference in time, with the notation: $\phi^n(x,y) \equiv \phi(x,y,t^n)$, with *n* being the time index. If we define the time step $\delta t^n \equiv t^{n+1} - t^n$ then the second order expression for the time derivative, centered about $t = t^{n+1/2}$, is $\delta t \dot{\phi}(x,y,t^{n+½}) \cong \phi^{n+1}(x,y) - \phi^n(x,y)$. By making use of the readily verified identity,

$$\nabla^2 \left[a,b\right] = \left[\nabla^2 a, b\right] + \left[a, \nabla^2 b\right] + 2\left[a_x, b_x\right] + 2\left[a_y, b_y\right], \tag{4}$$

straightforward manipulation gives the following set of equations relating the variables at time level *n+1* to those at time level *n*:

$$\left\{\nabla^2 - \theta\delta t L_{11}^{1v} - (\theta\delta t)^2 L_{11}^{2v}\right\}\phi^{n+1} = \left\{\nabla^2 - \theta\delta t L_{11}^{1v} + \delta t L_{11}^{3v} - \theta(\theta-1)(\delta t)^2 L_{11}^{2v}\right\}\phi^n + \theta(\delta t)^2 R_1^{2v} + \delta t R_1^{1v} \tag{5a}$$

$$\begin{aligned}
&\left\{-(\theta\delta t)L_{21}^{1v} - (\theta\delta t)^2 L_{21}^{2v}\right\}\phi^{n+1} + \left\{1 - \theta\delta t L_{22}^{1v} - (\theta\delta t)^2 L_{22}^{2v}\right\}V_z^{n+1} = \\
&\quad \left\{-\theta\delta t L_{21}^{1v} + \delta t L_{21}^{3v} - \theta(\theta-1)(\delta t)^2 L_{21}^{2v}\right\}\phi^n + \left\{1 - \theta\delta t L_{22}^{1v} + \delta t L_{22}^{3v} - \theta(\theta-1)(\delta t)^2 L_{22}^{2v}\right\}V_z^n \\
&\quad + \theta(\delta t)^2 R_2^{2v} + \delta t R_2^{1v}
\end{aligned} \tag{5b}$$

$$\left\{1 - \theta\delta t L_{11}^{1p}\right\}\psi^{n+1} - \theta\delta t L_{12}^{1p} I^{n+1} = \left\{1 + (1-\theta)\delta t L_{11}^{1p}\right\}\psi^n - \theta\delta t L_{12}^{1p} I^n + \delta t R_1^{1p} \tag{5c}$$

$$-\theta\delta t L_{21}^{1p}\psi^{n+1} + \left\{1 - \theta\delta t L_{22}^{1p}\right\} I^{n+1} = -\theta\delta t L_{21}^{1p}\psi^n + \left\{1 + (1-\theta)\delta t L_{22}^{1p}\right\} I^n + \delta t R_2^{1p} \tag{5d}$$

Here, we have defined the operators:

$$\begin{aligned}
L_{11}^{1v}\left\{\phi^{n+1}\right\} &= \left[\phi^{n+1}, \nabla^2\phi\right] + \left[\phi, \nabla^2\phi^{n+1}\right] + \mu\nabla^4\phi^{n+1} \\
L_{11}^{2v}\left\{\phi^{n+1}\right\} &= \left[\left[\phi^{n+1}, \nabla^2\psi\right], \psi\right] + \left[\left[\nabla^2\phi^{n+1}, \psi\right], \psi\right] + \left[\nabla^2\psi, \left[\phi^{n+1}, \psi\right]\right] \\
&\qquad + 2\left[\left[\phi_x^{n+1}, \psi_x\right], \psi\right] + 2\left[\left[\phi_y^{n+1}, \psi_y\right], \psi\right] \\
L_{11}^{3v}\left\{\phi^n\right\} &= \left[\phi, \nabla^2\phi\right] + \mu\nabla^4\phi \\
R_1^{2v} &= d_i\left[\left[\nabla^2\psi, I\right], \psi\right] + d_i\left[\left[\psi, \nabla^2 I\right], \psi\right] + d_i\left[\nabla^2\psi, \left[\psi, I\right]\right] \\
&\qquad + 2d_i\left[\left[\psi_x, I_x\right], \psi\right] + 2d_i\left[\left[\psi_y, I_y\right], \psi\right] \\
R_1^{1v} &= \left[\nabla^2\psi, \psi\right]
\end{aligned} \tag{6a}$$

$$
\begin{aligned}
L_{21}^{1v}\left\{\phi^{n+1}\right\} &= \left[\phi^{n+1}, V_z\right] \\
L_{21}^{2v}\left\{\phi^{n+1}\right\} &= \left[\left[\phi^{n+1}, I\right], \psi\right] + \left[I, \left[\phi^{n+1}, \psi\right]\right] \\
L_{22}^{1v}\left\{V_z^{n+1}\right\} &= \left[\phi, V_z^{n+1}\right] + \mu\nabla^2 V_z^{n+1} \\
L_{22}^{2v}\left\{V_z^{n+1}\right\} &= \left[\left[V_z^{n+1}, \psi\right], \psi\right] \\
L_{21}^{3v}\left\{\phi^{n}\right\} &= \tfrac{1}{2}\left[\phi, V_z\right] \\
L_{22}^{3v}\left\{V_z^{n}\right\} &= \tfrac{1}{2}\left[\phi, V_z\right] + \mu\nabla^2 V_z - \mu h\nabla^4 V_z \\
R_2^{2v} &= d_i\left[\left[\nabla^2\psi, \psi\right], \psi\right] + d_i\left[I, \left[\psi, I\right]\right] \\
R_2^{1v} &= \left[I, \psi\right]
\end{aligned}
\tag{6b}
$$

$$
\begin{aligned}
L_{11}^{1p}\left\{\psi^{n+1}\right\} &= \left[\phi, \psi^{n+1}\right] + d_i\left[\psi^{n+1}, I\right] + \eta\nabla^2\psi^{n+1} - \nu\nabla^4\psi^{n+1} \\
L_{12}^{1p}\left\{I^{n+1}\right\} &= d_i\left[\psi, I^{n+1}\right] \\
R_1^{1p} &= \theta\left[\phi^{n+1} - \phi^{n}, \psi\right] \\
L_{21}^{1p}\left\{\psi^{n+1}\right\} &= d_i\left[\nabla^2\psi^{n+1}, \psi\right] + d_i\left[\nabla^2\psi, \psi^{n+1}\right] + \left[V_z, \psi^{n+1}\right] \\
L_{22}^{1p}\left\{I^{n+1}\right\} &= \left[\phi, I^{n+1}\right] + \eta\nabla^2 I^{n+1} - \nu\nabla^4 I^{n+1} \\
R_2^{1p} &= +\theta\left\{\left[\phi^{n+1} - \phi^{n}, I\right] + \left[V_z^{n+1} - V_z^{n}, \psi\right]\right\} + d_i\left[\nabla^2\psi, \psi\right] + \left[V_z, \psi\right]
\end{aligned}
\tag{6c}
$$

We next represent each of the unknown scalar fields as a set of time-varying amplitudes multiplying time-independent spatial basis functions [2]. The domain is divided into M triangular regions. Within each triangle m, 18 basis functions are defined, $\left\{\nu_{m,i}(x, y); i = 1,18\right\}$ with the properties: (i) each of the basis functions is a quintic polynomial in (x,y) that has the value unity at one node for either the function or one of its first five derivatives, (ii) the basis function and its first five derivatives are zero at the two other nodes, and (iii) the quintic terms in the polynomial are constrained so that the normal derivative of the basis function is at most a cubic function along each side of the triangle. These conditions are enough to uniquely determine the 21 polynomial coefficients for each basis function and to insure that any scalar field represented in terms of these basis functions will have continuous first derivatives across triangle boundaries. This property is denoted in the literature by C^1 [9].

Using these basis functions, the unknown quantities take the physical significance of being the function, its two first, and three second derivatives at each of the nodes. For example, the stream function is represented as a sum over each of the 18 basis functions in each of the M triangles:

$$
\phi^n(x, y) = \sum_{m=1}^{M}\sum_{i=1}^{18}\nu_{m;i}(x, y)\Phi_{m;i}^n \tag{7}
$$

The unknowns $\left\{\Phi_i^n; i=1,18\right\}$ for triangle *m* break into three sets of six: $\left\{\Phi_{m,i}^n; i=1,6\right\}$ correspond to $\phi, \phi_x, \phi_y, \phi_{xx}, \phi_{xy}, \phi_{yy}$ at the first node, $\left\{\Phi_{m,i}^n; i=7,12\right\}$ are the same quantities at the second node, and $\left\{\Phi_{m,i}^n; i=13,18\right\}$ are these quantities at the third node. Note that all the unknowns in Eq. (7) are located at the nodes and are thus shared with all triangles using that node. Since there are asymptotically an average of six triangles utilizing each node, there are approximately a total of $3\times M$ unknowns for the global representation of each scalar field, rather than $18\times M$, which might be inferred from Eq. (7).

The discrete expansion (7) for each of the four scalar fields is substituted into the four equations (5). The Galerkin method consists of multiplying each equation (5a)-(5d) by each of the basis functions (or trial functions) and integrating these over the domain to obtain matrix equations for the discrete unknowns. Integration by parts is used to shift derivatives onto the trial functions so that no higher than second spatial derivatives appear in the final integrals. These are allowable in this procedure since the basis functions were constructed to have continuous first derivatives across triangle boundaries.

We next represent each quantity as the sum of an equilibrium part that is independent of time and a perturbed part, thus $\Phi^n \rightarrow \Phi^0 + \Phi^n$, etc. This yields the two sets of matrix equations that can be solved sequentially**:**

$$\begin{bmatrix} S_{11}^v & 0 \\ S_{21}^v & S_{22}^v \end{bmatrix} \begin{bmatrix} \Phi_{m;i}^{n+1} \\ V_{zm,i}^{n+1} \end{bmatrix} = \begin{bmatrix} D_{11}^v & 0 \\ D_{21}^v & D_{22}^v \end{bmatrix} \begin{bmatrix} \Phi_{m;i}^{n} \\ V_{zm,i}^{n} \end{bmatrix} + \begin{bmatrix} R_{11}^v & R_{12}^v \\ R_{21}^v & R_{22}^v \end{bmatrix} \begin{bmatrix} \Psi_{m;i}^{n} \\ I_{m,i}^{n} \end{bmatrix} \tag{8}$$

$$\begin{bmatrix} S_{11}^p & S_{12}^p \\ S_{21}^p & S_{22}^p \end{bmatrix} \begin{bmatrix} \Psi_{m;i}^{n+1} \\ I_{zm,i}^{n+1} \end{bmatrix} = \begin{bmatrix} D_{11}^p & D_{12}^p \\ D_{21}^p & D_{22}^p \end{bmatrix} \begin{bmatrix} \Psi_{m;i}^{n} \\ I_{zm,i}^{n} \end{bmatrix} + \begin{bmatrix} R_{11}^p & 0 \\ R_{21}^p & R_{22}^p \end{bmatrix} \begin{bmatrix} \Phi_{m;i}^{n+1} \\ V_{zm,i}^{n+1} \end{bmatrix} + \begin{bmatrix} Q_{11}^p & 0 \\ Q_{21}^p & Q_{22}^p \end{bmatrix} \begin{bmatrix} \Phi_{m;i}^{n} \\ V_{zm,i}^{n} \end{bmatrix} \tag{9}$$

The block matrix elements appearing here are defined in Appendix B. The matrix equations (8) and (9) are solved sequentially using the distributed version of the direct sparse matrix software package SuperLU [10]. This solution procedure is exceptionally efficient for a linear system, since only a one-time LU decomposition of the two matrices appearing on the left of the equals sign is required. A nonlinear problem requires performing the LU decomposition whenever there is significant change in the values of the matrix elements.

IV. Numerical Stability

The split semi-implicit time advance method given by equations (8) and (9) is based on advancing the velocity variables first each time step, followed by advancing the field variables. This clearly leads to a more efficient numerical method than if the coupled system were advanced together (as in Appendix C), since the rank of each matrix appearing on the left in Eq. (9) is half of what it would be for the combined system. To understand how this leads to an unconditionally stable time advance, let us consider a simpler problem that has the essential features of the one under investigation.

Consider the simplified Hall MHD system for the fluid velocity $\vec{V}$, the perturbed magnetic field $\vec{B}$, and the perturbed current density $\vec{J} = \nabla \times \vec{B}$. Assume for simplicity that the equilibrium magnetic field is uniform and in the $\hat{z}$ direction, and that the density is spatially constant. In suitably normalized units, the linearized momentum equation and the curl of the induction equation become simply:

$$\frac{\partial \vec{V}}{\partial t} = \vec{J} \times \vec{B}_0 \tag{10a}$$

$$\frac{\partial \vec{J}}{\partial t} = \nabla \times \frac{\partial \vec{B}}{\partial t} = \nabla \times \nabla \times \left[(\vec{V} - d_i \vec{J}) \times \vec{B}_0 \right] \tag{10b}$$

Setting $\vec{B}_0 = \hat{z}$, and specializing for simplicity to wave propagation in the $\hat{z}$ direction so that $\nabla \to \hat{z}\dfrac{\partial}{\partial z} \equiv \hat{z}\partial_z$, and both $\vec{J}$ and $\vec{V}$ are in the $\hat{x} - \hat{y}$ plane, the split semi-implicit time advance corresponding to equations (5) is

$$\left[1 - (\theta\delta t)^2 \nabla^2\right](\vec{V}^{n+1} - \vec{V}^n) = \delta t \left\{ \theta\delta t \left[\nabla^2 \vec{V}^n - d_i \nabla^2 \vec{J}^n \right] \right\} - \delta t \hat{z} \times \vec{J}^n \tag{11a}$$

$$\left[1 + \theta\delta t d_i \hat{z} \times \nabla^2\right](\vec{J}^{n+1} - \vec{J}^n) = \delta t \hat{z} \times \nabla^2 [\theta \vec{V}^{n+1} + (1-\theta)\vec{V}^n] - \delta t d_i \hat{z} \times \nabla^2 \vec{J}^n \tag{11b}$$

Or, in matrix component form:

$$\begin{aligned}
&\begin{bmatrix} 1-(\theta\delta t)^2\partial_z^2 & 0 & 0 & 0 \\ 0 & 1-(\theta\delta t)^2\partial_z^2 & 0 & 0 \\ 0 & \theta\delta t\partial_z^2 & 1 & -\theta\delta t d_i\partial_z^2 \\ -\theta\delta t\partial_z^2 & 0 & \theta\delta t d_i\partial_z^2 & 1 \end{bmatrix} \bullet \begin{bmatrix} V_x \\ V_y \\ J_x \\ J_y \end{bmatrix}^{n+1} \\
&= \begin{bmatrix} 1-\theta(\theta-1)(\delta t)^2\partial_z^2 & 0 & -\theta(\delta t)^2 d_i\partial_z^2 & \delta t \\ 0 & 1-\theta(\theta-1)(\delta t)^2\partial_z^2 & -\delta t & -\theta(\delta t)^2 d_i\partial_z^2 \\ 0 & (\theta-1)\delta t\partial_z^2 & 1 & -(\theta-1)\delta t d_i\partial_z^2 \\ -(\theta-1)\delta t\partial_z^2 & 0 & (\theta-1)\delta t d_i\partial_z^2 & 1 \end{bmatrix} \bullet \begin{bmatrix} V_x \\ V_y \\ J_x \\ J_y \end{bmatrix}^{n}
\end{aligned} \tag{12}$$

The numerical stability is determined by replacing the spatial derivative by an effective wave number, $\nabla^2 = \partial_z^2 \to -k_{eff}^2$, and by introducing the amplification factor r for the vector in Eq. (12). The amplification factor is thus determined by the generalized eigenvalue equation

$$\det\begin{bmatrix} 1-r+\theta(\delta t)^2 k_{eff}^2 s & 0 & \theta(\delta t)^2 d_i k_{eff}^2 & \delta t \\ 0 & 1-r+\theta(\delta t)^2 k_{eff}^2 s & -\delta t & \theta(\delta t)^2 d_i k_{eff}^2 \\ 0 & -\delta t k_{eff}^2 s & -r & -d_i \delta t k_{eff}^2 s \\ \delta t k_{eff}^2 s & 0 & -d_i \delta t k_{eff}^2 s & -r \end{bmatrix} = 0 \quad , \tag{13}$$

with $s \equiv [(1-r)\theta - 1]$. Evaluation of Eq. (13) with both a generalized eigenvalue solver and by symbolic expansion of the determinant and using a polynomial root finder give identical results: the amplification factor $|r| \le 1$, and thus the system is stable, for arbitrary real $k_{eff}^2 > 0$, $\delta t > 0$, and $d_i > 0$ provided the implicit parameter satisfies $\theta \ge 1/2$.

V. The Tilting Cylinder

Here we apply the method to the extension of the analysis of the tilting cylinder problem considered in [2] to the 4-field model. Following [2,11,12] we define an initial force free bipolar vortex equilibrium state:

$$\psi^0(x,y)=\begin{cases}\left[2/kJ_0(k)\right]J_1(kr)\cos\theta, & r<1,\\ (r-1/r)\cos\theta, & r>1,\end{cases}\qquad J_1(k)=0 \tag{14}$$

We have defined a polar coordinate system such that $y=r\cos\theta$, $x=r\sin\theta$. The initial toroidal field is defined as:

$$I^0(x,y)=\begin{cases}\sqrt{k^2\psi^2(x,y)+B_0^2} & r<1\\ B_0 & r>1\end{cases} \tag{15}$$

It is readily verified that these satisfy the equilibrium condition:

$$\nabla^2\psi^0+\tfrac{1}{2}\frac{dI^{02}}{d\psi}=0.$$

This equilibrium is known to be unstable to a tilting motion.

As in [2], the simulation box is a square with sides of length 4 that is divided into $(N\text{-}1)\times(N\text{-}1)$ rectangular regions, each with 2 right triangles (using the diagonal that runs from upper right to lower left). Conducting, no slip boundary conditions are applied at the walls. Thus, at the y boundary, we impose:

$$\psi=\frac{\partial\psi}{\partial x}=\frac{\partial^2\psi}{\partial x^2}=0,\ I=\frac{\partial I}{\partial x}=\frac{\partial^2 I}{\partial x^2}=0,$$
$$V_z=\frac{\partial V_z}{\partial x}=\frac{\partial^2 V_z}{\partial x^2}=0,\ \phi=\frac{\partial\phi}{\partial x}=\frac{\partial^2\phi}{\partial x^2}=\frac{\partial\phi}{\partial y}=\frac{\partial^2\phi}{\partial x\partial y}=0,$$

with similar, but rotated boundary conditions applied at the x-boundary.

We used uniform values of $\eta=\mu=0.001$, $h=1$, $\nu=(\Delta x)^2\eta$. The instability is known to persist even at $\eta=0$ and is thus considered an ideal instability. To examine the effect of the Hall term on this mode, we specify a value of the ion skin depth d_i and run the code in a linear mode to calculate the linear growth rate. Figure 1 gives this growth rate as a function of the square of d_i , for which it is seen to have a near linear dependence. Results for both $N=15$ and $N=31$ are shown. This study was performed with time-step $\Delta t=0.05$, but the growth rates changed by less than 2% when going from this value to $\Delta t=0.20$. The corresponding eigenmode for the case with $N=31$ and $d_i=0.2$ is shown in Fig. 2 (a)-(d) where we display contours of the perturbed values of the magnetic flux ψ with range [-0.0229,+0.0229], the stream function ϕ with range [0.0076,+0.0175], the z-directed magnetic field I with range [-0.073, +0.072], and the z-component of the velocity, $V_{z,}$, with range [-0.0175,+0.0175].

VI. Harris Reconnection

We define a Harris equilibrium and perturbation similar to the one used in the GEM magnetic reconnection challenge [13], but within the limitations of the 4-field equations. The initial equilibrium, shown in Fig. 3, is defined by an equilibrium and a perturbed magnetic flux function as follows:

$$\psi^0\left(x,y\right)=\frac{1}{2}\log\left(\cosh 2y\right); \qquad \psi\left(x,y\right)=\varepsilon\cos k_x x\cos k_y y \tag{16}$$

with all the other quantities initialized to zero. The initial equilibrium and perturbed current densities are just the laplacian of the flux, $J^0=\nabla^2\psi^0, J=\nabla^2\psi,$ The computation is carried out in a rectangular domain $-L_x/2\le x\le L_x/2$ and $-L_y/2\le y\le L_y/2$. The system is taken to be periodic in the x direction with ideal conducting boundaries (see Sec. V) at $y=\pm L_y/2$. As in [11], we chose the parameters such that $k_x=2\pi/L_x$, $k_y=\pi/L_y$, with $L_x=25.6, L_y=12.8, \varepsilon=0.1$.

We illustrate the results from a pair of comparison calculations in Figs. 3-7 . Both cases had $N=31$, $\eta=\mu=0.001$, $h=1$, $\nu=(\Delta x)^2\eta$, time step $\Delta t=0.25$, implicit parameter $\theta=0.6$. The first case had the ion skin depth set to zero, $d_i=0$, while the second case had $d_i=1.0$.

Figures 4 and 5 show the poloidal magnetic flux (top) and current density (bottom) for the two cases at time $t=37.5$. We see in Fig. 4 that the case with $d_i=0$ (resistive MHD) has a thin current layer on the midplane, known as the Sweet-Parker [14]layer. The corresponding case with $d_i=1.0$ (Hall-MHD) is shown in Figs. 5-6. In comparing Fig. 4 and Fig. 5, we see that the Sweet-Parker layer is much shorter with $d_i=1$, and the reconnection region has essentially changed character from a Y-point to an X-point as expected[15]. In Fig. 6 we see the out of plane (z-directed) velocity (top) and magnetic field (bottom) in the Hall-reconnection case with $d_i=1$. Large in-out flows develop as a result of the reconnecting fields. The magnetic field forms the characteristic quadrupole structure near the midplane.

In Figure 7 we show a comparison of the amount of reconnected flux (dark curves) and the reconnection rates (red curves) vs time for the two cases. It is seen that the Hall reconnection case with $d_i=1.0$ causes reconnection to occur about 8 times faster that the resistive MHD case with $d_i=0$ for these parameters.

VII. The Taylor Problem

The Taylor problem [3] consists of an initial magnetic field given by the flux function

$$\psi^0(y) = -\tfrac{1}{2}y^2 \tag{17}$$

The initial z-component of the magnetic field, $I^0(x,y)$, is initially zero, as are the velocity variables ϕ^0 and V_z^0. For times $t \geq 0$, the top and bottom boundaries are perturbed as follows:

$$\begin{aligned} \psi(x,\pm 1) &= \varepsilon(t)\cos(kx) \\ \phi(x,\pm 1) &= \mp\frac{1}{k}\dot{\varepsilon}(t)\sin(kx) \end{aligned} \tag{18}$$

The left and right boundaries are periodic. The time dependent perturbation function is defined as

$$\varepsilon(t) = \varepsilon^0\left[1 - \left(1 + t/\tau\right)\exp(-t/\tau)\right] \tag{19}$$

This problem has been studied both theoretically [16] and numerically [17] for the case of resistive MHD ($d_i=0$), but only numerical results [3] exist for the “2-fluid” or “Hall MHD” case of non-zero d_i. As in these earlier studies, we define the *reconnected magnetic flux* as: $\Psi(t) = ½[\psi(0,0,t) - \psi(L_x/2,0,t)]$, and the *reconnection rate* as the time derivative of this.

The results of a series of calculations with $\varepsilon^0=.01$, $\tau=1.0$, $k=2\pi/L_x$, $\eta=\mu=10^{-4}$, $h=1$, are presented in Fig. 8. The reconnected flux (top) and reconnection rate (bottom) vs. time are shown for different values of the collisionless ion skin depth d_i. The parameter d_i is seen to have a significant impact on the reconnection rate, especially at early time. These results are seen to be qualitatively similar to Fig. 1 of Ref. [3], but extend those results to a nonlinear regime with a larger perturbation amplitude. More generally, the fact that d_i ,or the Hall term, can greatly accelerate the rate of forced magnetic reconnection is consistent with results reported in earlier studies.

The calculations presented in Fig. 8 were performed on a domain with $L_x=8$, $L_y=2$, that was broken up into 30×30 rectangles, each divided into 2 triangles with a line from upper right to lower left. The other numerical parameters used were $\delta t=0.5$ and $\theta=0.6$. As in the other studies in this paper, there was no attempt to concentrate resolution in the reconnection layer, although this could dramatically increase the efficiency of this method and will be pursued in future studies.

VIII. Summary and Discussion

A new technique for solving the extended MHD equations has been described and applied to the 4-field model. This is a generalization of Appendix D of [2] where the MHD 2-field model was discussed. The further generalization of this method to the fully compressible 6-field or 8-field system of the full extended MHD equations is underway.

The method is characterized by representing the fluid and field in a potential/stream-function representation [1] in which higher derivatives occur. The higher derivatives are handled by using a compact triangular high-order finite element representation with C^1 continuity rather than by introducing auxiliary variables that would increase the rank of the matrices.

The split semi-implicit time advance is introduced that breaks the time advance into two steps each cycle. In the first step, the implicit method avoids time-step restrictions due to the Alfven waves by inverting the ideal MHD force operator. In the second step, the implicit field advance avoids time-step restrictions due to the dispersive waves. It was shown in Sec. IV that the combined 2-step time advance is unconditionally stable for arbitrary time step as long as the implicitness parameter θ is greater than ½. The relatively small matrices that need to be inverted make a direct sparse matrix inversion practical. A side benefit is that for linear problems, the LU decomposition only needs to be performed once, making the method exceptionally efficient.

The present work demonstrated the validity of this method by calculating the effects of the collisionless ion skin depth on the ideal MHD tilt mode, and on the rate of magnetic reconnection for both a self-reconnecting and a forced reconnection system. Future work will extend this to a higher order system of equations, to toroidal geometry, and to three dimensions.

Finally we remark that we did not take advantage of the geometrical flexibility that is offered by triangles in the applications presented here. Triangular elements offer the potential to fit complex domain boundaries and to easily add refinement where needed, and this will be exploited in future studies.

Acknowledgements

The authors benefited from many useful discussions with their colleagues: J. Chen, P. Fischer, G. Fu, W. Park, R. Samtaney, C. Sovinec, H. Strauss, and L. Sugiyama in particular. This work was supported by US DoE contract DE-AC02-76CH03073 and by the DOE SciDAC Center for Extended Magnetohydrodynamic Modeling.

Appendix A: Definitions and symmetry relations.

The matrix and tensor quantities used in the text are defined as follows. These are evaluated by closed form integration of the local polynomial expansions as described in Appendices B and D of [2].

$$D_{i,j}\Phi_j \equiv \iint v_i(\xi,\eta)\phi(\xi,\eta)d\xi d\eta$$

$$A_{i,j}\Phi_j \equiv \iint v_i(\xi,\eta)\nabla^2\phi(\xi,\eta)d\xi d\eta$$

$$B_{i,j}\Phi_j \equiv \iint v_i(\xi,\eta)\nabla^4\phi(\xi,\eta)d\xi d\eta$$

$$G_{i,j,k}\Psi_j\Phi_k \equiv \iint v_i(\xi,\eta)\left[\nabla^2\psi,\phi\right]d\xi d\eta = -G_{k,j,i}\Psi_j\Phi_k$$

$$K_{i,j,k}\Psi_j\Phi_k \equiv \iint v_i(\xi,\eta)\left[\psi,\phi\right]d\xi d\eta = -K_{i,k,j}\Psi_j\Phi_k$$

$$P_{i,j,k,l}\Psi_j\Phi_k Z_l \equiv \iint v_i(\xi,\eta)\left[\left[\phi,\nabla^2\psi\right],\zeta\right]d\xi d\eta = -P_{l,j,k,i}\Psi_j\Phi_k Z_l$$

$$(note: P_{k,j,i,l}\Psi_j\Phi_k Z_l = \iint v_i(\xi,\eta)\left[\nabla^2\psi,\left[\zeta,\phi\right]\right]d\xi d\eta = -P_{l,j,i,k}\Psi_j\Phi_k Z_l)$$

$$\begin{aligned} Q_{i,j,k,l}\Phi_j\Psi_k Z_l &\equiv \iint v_i(\xi,\eta)\left[\left[\phi,\psi\right],\zeta\right]d\xi d\eta = -Q_{i,k,j,l}\Phi_j\Psi_k Z_l \\ &= -Q_{l,j,k,i}\Phi_j\Psi_k Z_l = Q_{l,k,j,i}\Phi_j\Psi_k Z_l \end{aligned}$$

$$\begin{aligned} R_{i,j,k,l}\Phi_j\Psi_k Z_l &\equiv \iint v_i(\xi,\eta)\left\{\left[\left[\phi_x,\psi_x\right],\zeta\right]+\left[\left[\phi_y,\psi_y\right],\zeta\right]\right\}d\xi d\eta \\ &= -R_{l,j,k,i}\Phi_j\Psi_k Z_l = -R_{i,k,j,l}\Phi_j\Psi_k Z_l = R_{l,k,j,i}\Phi_j\Psi_k Z_l \end{aligned}$$

$$D_{i,j}J_j \equiv A_{i,j}\Psi_j$$

$$C^0_{i,j,k,l} \equiv \begin{bmatrix} P_{k,j,i,l} - P_{i,j,k,l} + P_{i,k,j,l} + 2R_{i,j,k,l} \\ P_{k,l,i,j} - P_{i,l,k,j} + P_{i,k,l,j} + 2R_{i,l,k,j} \end{bmatrix}$$

$$\bar{G}_{i,j,k} \equiv (G_{i,k,j} + G_{i,j,k})$$

$$\bar{Q}_{i,j,k,l} \equiv \tfrac{1}{2}\left(Q_{i,j,k,l} + Q_{i,j,l,k}\right)$$

Appendix B: The Matrix Elements

Making use of the definitions and symmetry relations in Appendix A, the matrix elements are given as follows:

$$S_{11}^{v}=\begin{Bmatrix} A_{i,j}+\theta\delta t\left[-\mu B_{i,j}+\bar{G}_{i,j,k}(\Phi_k+\Phi_k^0)\right] \\ +(\theta\delta t)^2 C_{i,k,j,l}^0 \tfrac{1}{2}(\Psi_k+\Psi_k^0)(\Psi_l+\Psi_l^0) \end{Bmatrix}$$

$$S_{21}^{v}=\begin{Bmatrix} -\theta\delta t K_{i,j,k}(V_{zk}+V_{zk}^0) \\ -(\theta\delta t)^2 Q_{i,j,k,l}\left[(I_k+I_k^0)(\Psi_l+\Psi_l^0)-(\Psi_k+\Psi_k^0)(I_l+I_l^0)\right] \end{Bmatrix}$$

$$S_{22}^{v}=\begin{Bmatrix} D_{i,j}-\theta\delta t\left[\mu(A_{i,j}-hB_{i,j})+K_{i,k,j}(\Phi_k+\Phi_k^0)\right] \\ -(\theta\delta t)^2\bar{Q}_{i,j,k,l}(\Psi_k+\Psi_k^0)(\Psi_l+\Psi_l^0) \end{Bmatrix}$$

$$D_{11}^{v}=\begin{Bmatrix} A_{i,j}+\delta t(1-\theta)\mu B_{i,j}+\delta t\bar{G}_{i,j,k}\left[\theta(\Phi_k+\Phi_k^0)-(\tfrac{1}{2}\Phi_k+\Phi_k^0)\right] \\ +\theta(\theta-1)(\delta t)^2 C_{i,k,j,l}^0\tfrac{1}{2}(\Psi_k+\Psi_k^0)(\Psi_l+\Psi_l^0) \end{Bmatrix}$$

$$D_{21}^{v}=\begin{Bmatrix} \delta t K_{i,j,k}\left[-\theta(V_{zk}+V_{zk}^0)+(\tfrac{1}{2}V_{zk}+V_{zk}^0)\right] \\ -\theta(\theta-1)(\delta t)^2 Q_{i,j,k,l}\left[(I_k+I_k^0)(\Psi_l+\Psi_l^0)-(\Psi_k+\Psi_k^0)(I_l+I_l^0)\right] \end{Bmatrix}$$

$$D_{22}^{v}=\begin{Bmatrix} D_{i,j}+\delta t\left[(1-\theta)\mu(A_{i,j}-hB_{i,j})+K_{i,k,j}\left[(\tfrac{1}{2}\Phi_k+\Phi_k^0)-\theta(\Phi_k+\Phi_k^0)\right]\right] \\ -\theta(\theta-1)(\delta t)^2\bar{Q}_{i,j,k,l}(\Psi_k+\Psi_k^0)(\Psi_l+\Psi_l^0) \end{Bmatrix}$$

$$R_{11}^{v}=\begin{Bmatrix} \delta t\bar{G}_{i,j,k}(\tfrac{1}{2}\Psi_k+\Psi_k^0)+\theta(\delta t)^2\eta G_{i,k,j}J_k \\ +\theta(\delta t)^2 d_i C_{i,j,k,l}^0\times\left[(I_k+I_k^0)(\tfrac{1}{2}\Psi_l+\Psi_l^0)\right] \end{Bmatrix}$$

$$R_{12}^{v}=\left\{\theta(\delta t)^2 d_i C_{i,k,j,l}^0\times\left[\tfrac{1}{2}\Psi_k^0\Psi_l^0\right]\right\}$$

$$R_{21}^{v}=\begin{Bmatrix} -\delta t K_{i,j,k}(\tfrac{1}{2}I_k+I_k^0) \\ +\theta(\delta t)^2\begin{pmatrix} -d_i\left[P_{i,j,k,l}+P_{i,k,j,l}+P_{i,l,k,j}\right]\times\left[\Psi_k^0\Psi_l^0+\tfrac{1}{2}\left(\Psi_k\Psi_l^0+\Psi_l\Psi_k^0\right)+\tfrac{1}{3}\Psi_k\Psi_l\right] \\ -d_iQ_{i,j,k,l}\left[I_k^0I_l^0+\tfrac{1}{2}\left(I_kI_l^0+I_lI_k^0\right)+\tfrac{1}{3}I_kI_l\right]+\eta(G_{i,k,j}-G_{i,j,k})(\tfrac{1}{2}I_k+I_k^0) \end{pmatrix} \end{Bmatrix}$$

$$R_{22}^{v}=\begin{Bmatrix} +\delta t K_{i,j,k}(\tfrac{1}{2}\Psi_k+\Psi_k^0) \\ +\theta(\delta t)^2\begin{pmatrix} \eta\left[(G_{i,j,k}-G_{i,k,j})(\tfrac{1}{2}\Psi_k+\Psi_k^0)\right] \\ -d_i\left[Q_{i,k,j,l}+Q_{i,k,l,j}\right]\times\left[\Psi_k^0I_l^0+\tfrac{1}{2}\left(\Psi_kI_l^0+I_l\Psi_k^0\right)+\tfrac{1}{3}\Psi_kI_l\right] \end{pmatrix} \end{Bmatrix}$$

$$S_{11}^{p}=\left\{D_{i,j}-\theta\delta t\left[\eta A_{i,j}-\nu B_{i,j}+K_{i,k,j}(\Phi_k+\Phi_k^0)+d_iK_{i,j,k}(I_k+I_k^0)\right]\right\}$$
$$S_{12}^{p}=-\theta\delta t d_iK_{i,k,j}(\Psi_k+\Psi_k^0)$$
$$S_{21}^{p}=-\theta\delta t\left[d_i\bar{G}_{i,j,k}(\Psi_k+\Psi_k^0)+K_{i,k,j}(V_{zk}+V_{zk}^0)\right]$$
$$S_{22}^{p}=\left\{D_{i,j}-\theta\delta t\left[K_{i,k,j}(\Phi_k+\Phi_k^0)+\eta A_{i,j}-\nu B_{i,j}\right]\right\}$$

$$D_{11}^{p}=\left\{D_{i,j}+\delta t\begin{bmatrix}(1-\theta)(\eta A_{i,j}-\nu B_{i,j})+K_{i,k,j}\left[-\theta(\Phi_k+\Phi_k^0)+\tfrac{1}{2}\Phi_k+\Phi_k^0\right]\\ +d_iK_{i,j,k}\left[-\theta(I_k+I_k^0)+\tfrac{1}{2}I_k+I_k^0\right]\end{bmatrix}\right\}$$
$$D_{12}^{p}=\delta t d_iK_{i,k,j}\left[-\theta(\Psi_k+\Psi_k^0)+\tfrac{1}{2}\Psi_k+\Psi_k^0\right]$$
$$D_{21}^{p}=\delta t\left\{\begin{matrix}d_i\bar{G}_{i,j,k}\left[-\theta(\Psi_k+\Psi_k^0)+\tfrac{1}{2}\Psi_k+\Psi_k^0\right]\\ +K_{i,k,j}\left[-\theta(V_{zk}+V_{zk}^0)+\tfrac{1}{2}V_{zk}+V_{zk}^0\right]\end{matrix}\right\}$$
$$D_{22}^{p}=\left\{D_{i,j}+\delta t\left[K_{i,k,j}\left\{-\theta(\Phi_k+\Phi_k^0)+\tfrac{1}{2}\Phi_k+\Phi_k^0\right\}+(1-\theta)(\eta A_{i,j}-\nu B_{i,j})\right]\right\}$$

$$R_{11}^{p}=\delta t\theta K_{i,j,k}(\Psi_k+\Psi_k^0)$$
$$R_{21}^{p}=\delta t\theta K_{i,j,k}(I_k+I_k^0)$$
$$R_{22}^{p}=\delta t\theta K_{i,j,k}(\Psi_k+\Psi_k^0)$$

$$Q_{11}^{p}=\delta tK_{i,j,k}\left[-\theta(\Psi_k+\Psi_k^0)+\tfrac{1}{2}\Psi_k+\Psi_k^0\right]$$
$$Q_{21}^{p}=\delta tK_{i,j,k}\left[-\theta(I_k+I_k^0)+\tfrac{1}{2}I_k+I_k^0\right]$$
$$Q_{22}^{p}=\delta tK_{i,j,k}\left[-\theta(\Psi_k+\Psi_k^0)+\tfrac{1}{2}\Psi_k+\Psi_k^0\right]$$

Appendix C: Alternate Formulation

Note that an algebraically simpler, but less efficient fully implicit system can also be formed as follows

$$\begin{bmatrix} S_{11}^v & 0 & R_{11}^v & 0 \\ S_{21}^v & S_{22}^v & R_{21}^v & R_{22}^v \\ R_{11}^p & 0 & S_{11}^p & S_{12}^p \\ R_{21}^p & R_{22}^p & S_{21}^p & S_{22}^p \end{bmatrix} \bullet \begin{bmatrix} \phi^{n+1} \\ V_z^{n+1} \\ \psi^{n+1} \\ I^{n+1} \end{bmatrix} = \begin{bmatrix} D_{11}^v & 0 & Q_{11}^v & 0 \\ D_{21}^v & D_{22}^v & Q_{21}^v & Q_{22}^v \\ Q_{11}^p & 0 & D_{11}^p & D_{12}^p \\ Q_{21}^p & Q_{22}^p & D_{21}^p & D_{22}^p \end{bmatrix} \bullet \begin{bmatrix} \phi^{n} \\ V_z^{n} \\ \psi^{n} \\ I^{n} \end{bmatrix} \quad (1.1)$$

This should be equivalent to the previous set, but will be more time consuming to invert since the single matrix will have twice the rank of each of the two matrices in Eqs. (8) and (9) .

Here,

$$S_{11}^v = \left\{ A_{i,j} - \theta\delta t\mu B_{i,j} + \theta\delta t(G_{i,j,k} + G_{i,k,j})(\Phi_k + \Phi_k^0) \right\}$$
$$S_{21}^v = -\theta\delta t K_{i,j,k}(V_k + V_k^0)$$
$$R_{11}^p = -\theta\delta t K_{i,j,k}(\Psi_k + \Psi_k^0)$$
$$R_{21}^p = -\theta\delta t K_{i,j,k}(I_k + I_k^0)$$

$$S_{22}^v = \left\{ D_{i,j} - \theta\delta t(\Phi_k + \Phi_k^0)K_{i,k,j} - \mu\theta\delta t A_{i,j} \right\}$$
$$R_{22}^p = -\theta\delta t K_{i,j,k}(\Psi_k + \Psi_k^0)$$

$$R_{11}^v = -\theta\delta t(G_{i,j,k} + G_{i,k,j})(\Psi_k + \Psi_k^0)$$
$$R_{21}^v = -\theta\delta t K_{i,k,j}(I_k + I_k^0)$$
$$S_{11}^p = \left\{ D_{i,j} - \theta\delta t(\Phi_k + \Phi_k^0)K_{i,k,j} - d_i\theta\delta t K_{i,j,k}(I_k + I_k^0) - \eta\theta\delta t A_{i,j} \right\}$$
$$S_{21}^p = \left\{ -d_i\theta\delta t(G_{i,j,k} + G_{i,k,j})(\Psi_k + \Psi_k^0) - \theta\delta t K_{i,k,j}(V_k + V_k^0) \right\}$$

$$R_{22}^v = -\theta\delta t K_{i,j,k}(\Psi_k + \Psi_k^0)$$
$$S_{12}^p = -d_i\theta\delta t K_{i,k,j}(\Psi_k + \Psi_k^0)$$
$$S_{22}^p = \left\{ D_{i,j} - \theta\delta t(\Phi_k + \Phi_k^0)K_{i,k,j} - \eta\theta\delta t A_{i,j} \right\}$$

$$D_{11}^{v} = \left\{A_{i,j} + (1-\theta)\delta t\mu B_{i,j} - \delta t(G_{i,j,k} + G_{i,k,j})[(\tfrac{1}{2}\Phi_k + \Phi_k^0) - \theta(\Phi_k + \Phi_k^0)\right\}$$
$$D_{21}^{v} = \delta t K_{i,j,k}[(\tfrac{1}{2}V_k + V_k^0) - \theta(V_k + V_k^0)]$$
$$Q_{11}^{p} = \delta t K_{i,j,k}[(\tfrac{1}{2}\Psi_k + \Psi_k^0) - \theta(\Psi_k + \Psi_k^0)]$$
$$Q_{21}^{p} = \delta t K_{i,j,k}[(\tfrac{1}{2}I_k + I_k^0) - \theta(I_k + I_k^0)]$$

$$D_{22}^{v} = \left\{D_{i,j} + \delta t K_{i,k,j}[(\tfrac{1}{2}\Phi_k + \Phi_k^0) - \theta(\Phi_k + \Phi_k^0)] + \mu(1-\theta)\delta t A_{i,j}\right\}$$
$$Q_{22}^{p} = \delta t K_{i,j,k}[(\tfrac{1}{2}\Psi_k + \Psi_k^0) - \theta(\Psi_k + \Psi_k^0)]$$

$$Q_{11}^{v} = \delta t(G_{i,j,k} + G_{i,k,j})[(\tfrac{1}{2}\Psi_k + \Psi_k^0) - \theta(\Psi_k + \Psi_k^0)]$$
$$Q_{21}^{v} = \delta t K_{i,k,j}[(\tfrac{1}{2}I_k + I_k^0) - \theta(I_k + I_k^0)]$$
$$D_{11}^{p} = \left\{D_{i,j} + \delta t K_{i,k,j}[(\tfrac{1}{2}\Phi_k + \Phi_k^0) - \theta(\Phi_k + \Phi_k^0)] + d_i\delta t K_{i,j,k}[(\tfrac{1}{2}I_k + I_k^0) - \theta(I_k + I_k^0)] + \eta(1-\theta)\delta t A_{i,j}\right\}$$
$$D_{21}^{p} = \left\{d_i\delta t(G_{i,j,k} + G_{i,k,j})[(\tfrac{1}{2}\Psi_k + \Psi_k^0) - \theta(\Psi_k + \Psi_k^0)] + \delta t K_{i,k,j}[(\tfrac{1}{2}V_k + V_k^0) - \theta(V_k + V_k^0)]\right\}$$

$$Q_{22}^{v} = \delta t K_{i,j,k}[(\tfrac{1}{2}\Psi_k + \Psi_k^0) - \theta(\Psi_k + \Psi_k^0)]$$
$$D_{12}^{p} = d_i\delta t K_{i,k,j}[(\tfrac{1}{2}\Psi_k + \Psi_k^0) - \theta(\Psi_k + \Psi_k^0)]$$
$$D_{22}^{p} = \left\{D_{i,j} + \delta t K_{i,k,j}[(\tfrac{1}{2}\Phi_k + \Phi_k^0) - \theta(\Phi_k + \Phi_k^0)] + \eta(1-\theta)\delta t A_{i,j}\right\}$$

References

[1] W. Park, E. V. Belova, G. Y. Fu, et al, Phys Plasmas **6** (1999) 1796-1803 Part 2
[2] S.C. Jardin, J. Comp. Phys. **200** (2004) 133-152
[3] R.Fitzpatrick, Phys Plasmas, **11** (2004) 937-946
[4] R. Hazeltine, M. Kotschenreuther, P. Morrison, Phys. Fluids **28** (1985) 2466
[5] D. Biscamp, E. Schwarz, and J. F. Drake, Phys. Plasmas **4,** 1002 (1997)
[6] B. N. Rogers, R. E. Denton, J. F. Drake, and M. A. Shay, Phys. Rev. Lett., **87** (2001) 19504-
[7] E. J. Caramana, J. Comp. Phys. **96** (1991) 484-493
[8] C. R. Sovinec, A. H. Glasser, G. A. Gianakon, et al, J. Comput Phys. **195**(2004) 355-386
[9] D. Braess, “Finite Elements”, Cambridge University Press (2001)
[10] J.W. Demmel, J.R. Gilbert, Y. S. Li, “SuperLU Users Guide”, U.C. Berkeley, October 2003
[11] H. R. Strauss and D. W. Longcope, J. Comput. Phys, **147**, 318-336 (1998)
[12] R. Richard, R. D. Sydora, and M. Ashour-abdalla, Phys. Fluids B **2**, 488 (1990)
[13] J. Birn, J.F. Drake, M. A. Shay, et al, Geophys. Res.:Space 106 (2001) 3715
[14] E. N. Parker, J. Geophys. Res. **62** (1957) 509
[15] D. Biskamp, E. Schwarz, J. F. Drake, Phys. Plas. **4** (1997) 1002
[16] T. S. Hahm and R. M. Kulsrud, Phys. Fluids **28**, 2412 (1985)
[17] R. Fitzpatrick, Phys. Plasmas **10**, 1782 (2003)

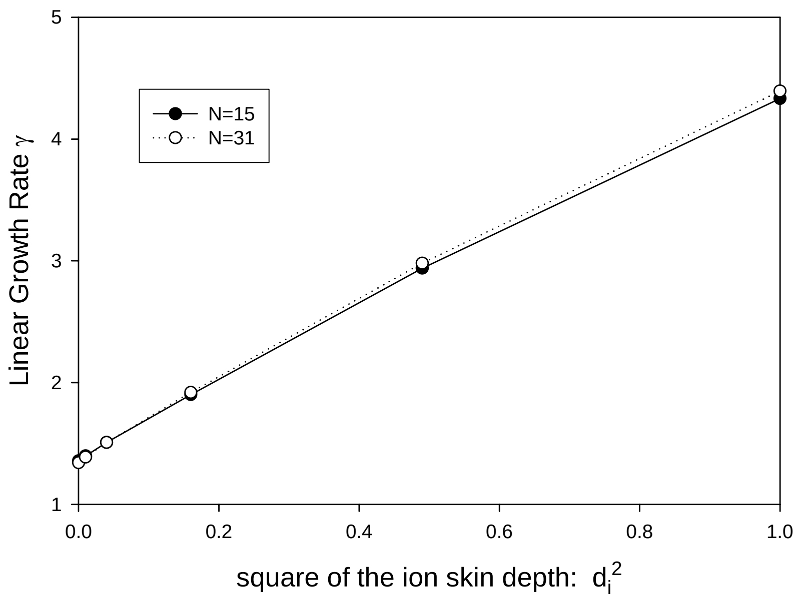

Figure 1: Dependence of the linear growth rate for the tilt mode on the square of the ion skin depth, d_i^2 Results are shown for calculations with 15×15 and 31×31 rectangles, each divided into 2 triangles.

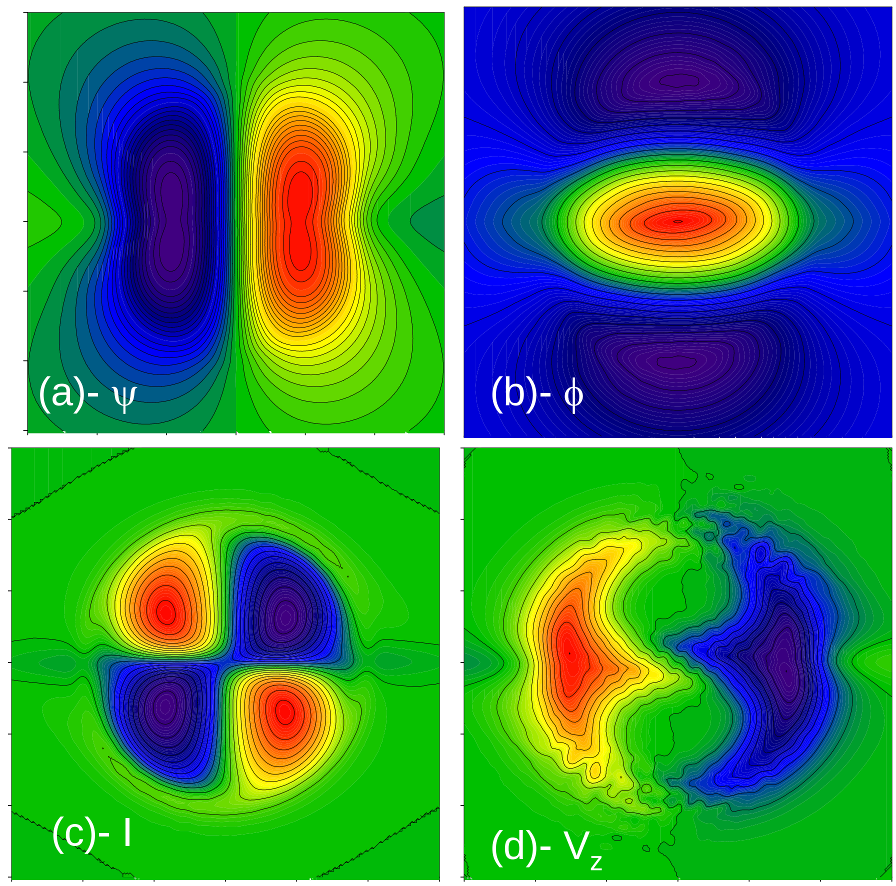

Figure 2: Linear eigenmodes for one of the calculations performed for Fig. 1 with $N=31$ and $d_i=0.2$. (a) contours of the perturbed values of the magnetic flux ψ with range [-0.0229,+0.0229], (b) the stream function φ with range [0.0076,+0.0175], the (c) z-directed magnetic field I with range [-0.073, +0.072], and (d) the z-component of the velocity, $V_{z,}$, with range [-0.0175,+0.0175]. The region (-1.5,1.5) ×(-1.5,1.5) is shown while the calculation was performed on a (-2.0,2.0) ×(-2.0,2.0) domain with conductor boundary conditions imposed.

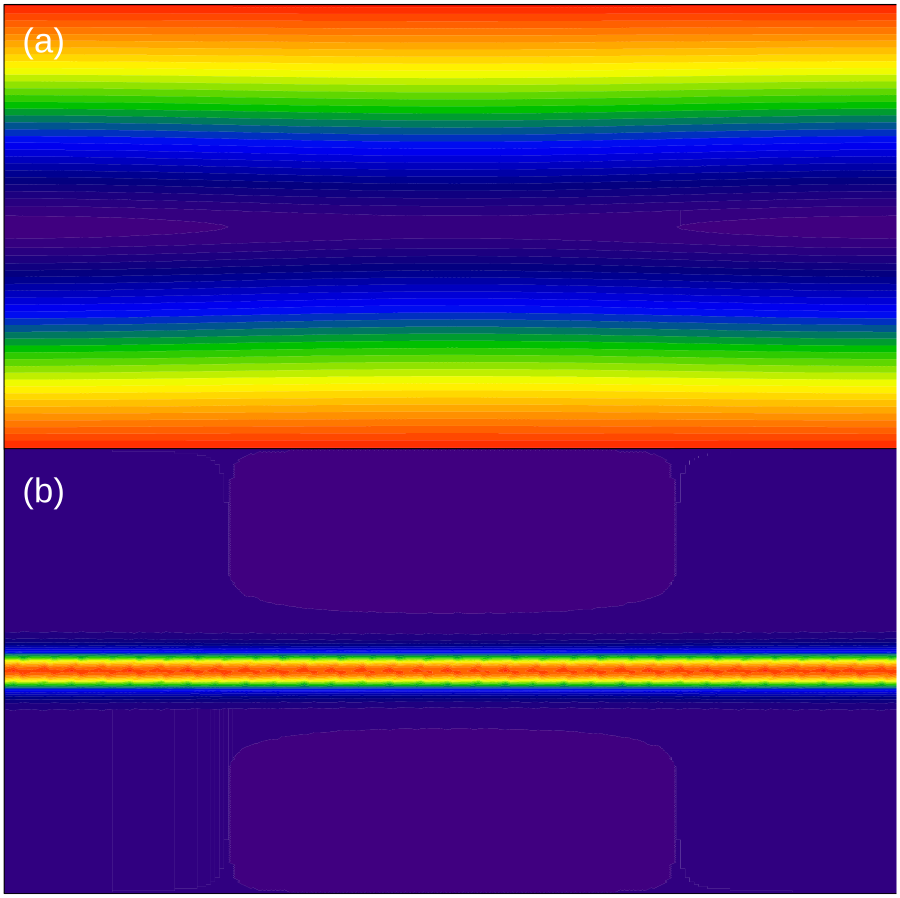

Figure 3: Initial equilibrium poloidal magnetic flux ψ (top) and current density J (bottom) for the Harris reconnection problem. The ranges of the data are (a) [-0.1, 6.054] and (b) [-0.00095, 2.189].

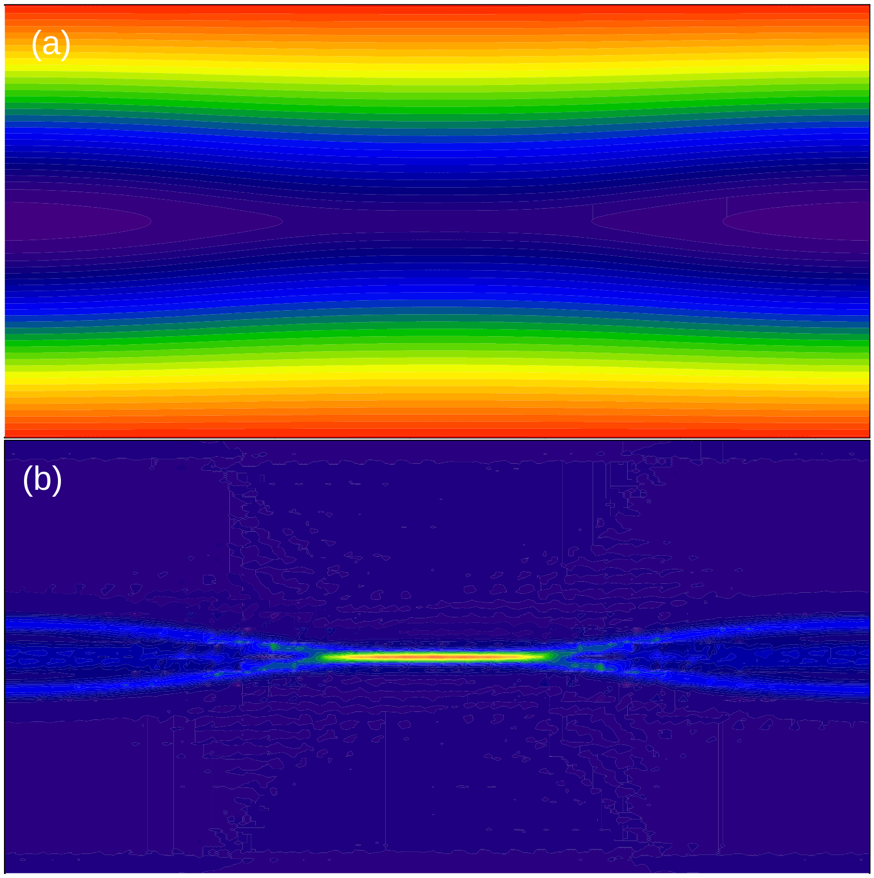

Figure 4: Poloidal magnetic flux (top) and current density (bottom) for the "resistive MHD" reconnection at time $t=37.5$ with $d_i=0$. Minimum and maximum values of the scalar fields are (a) [-0.1426,6.0535], and (b) [-0.576,5.820].

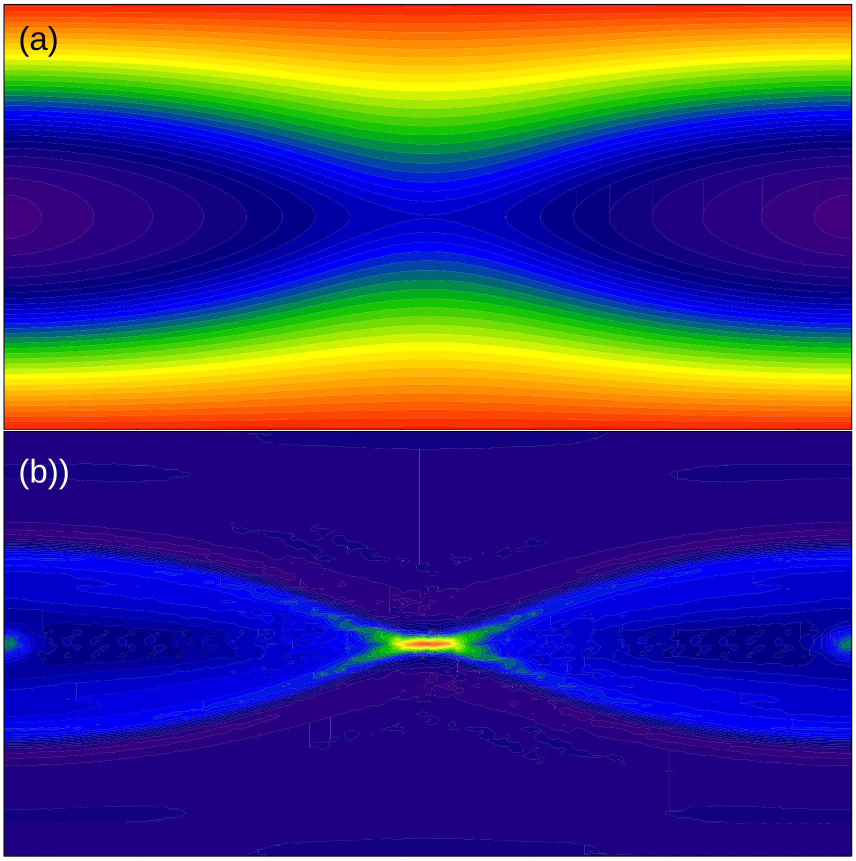

Figure 5: Poloidal magnetic flux (top) and current density (bottom) for the "Hall- MHD" reconnection at time *t=37.5* with $d_i=1.0$. Minimum and maximum values of the scalar fields are (a) [--0.337,6.0535], and (b) [-0.312,2.935].

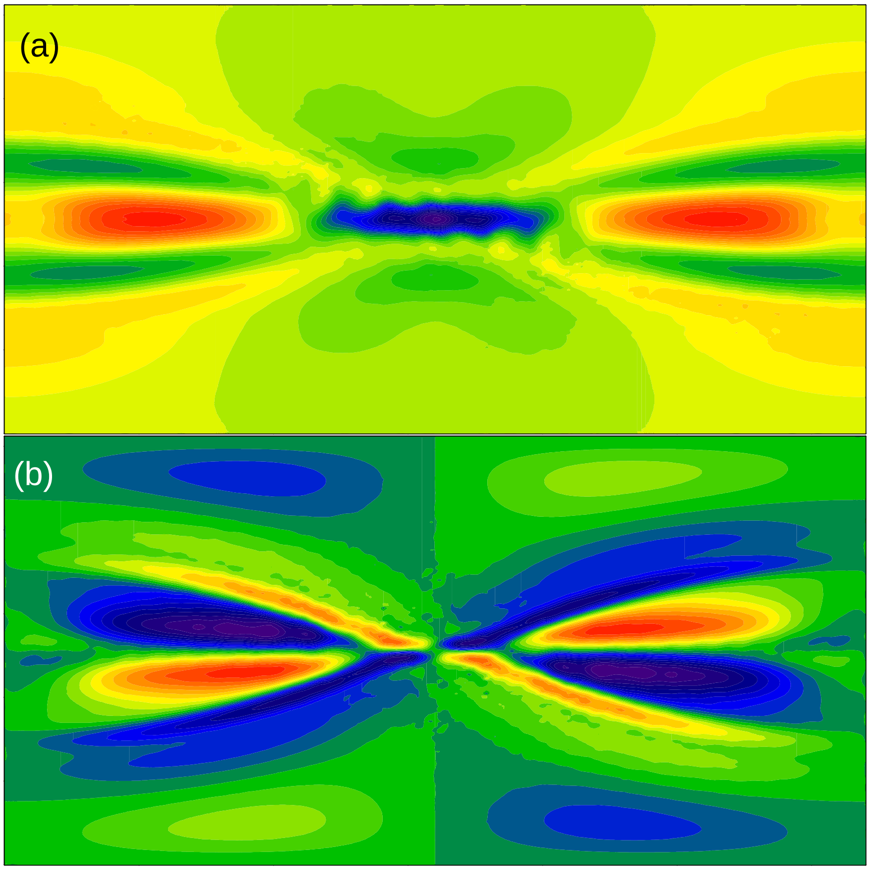

Figure 6: Out of plane (*z*-directed) velocity (top) and magnetic field in the Hall-reconnection case with $d_i=1$ (bottom). Large in-out flows develop as a result of the reconnecting fields. The magnetic field forms the characteristic quadrupole structure near the midplane. Min and max. values of the scalar fields are (a) [-0.388, 0.210] and (b) [-0.108, 0.1075].

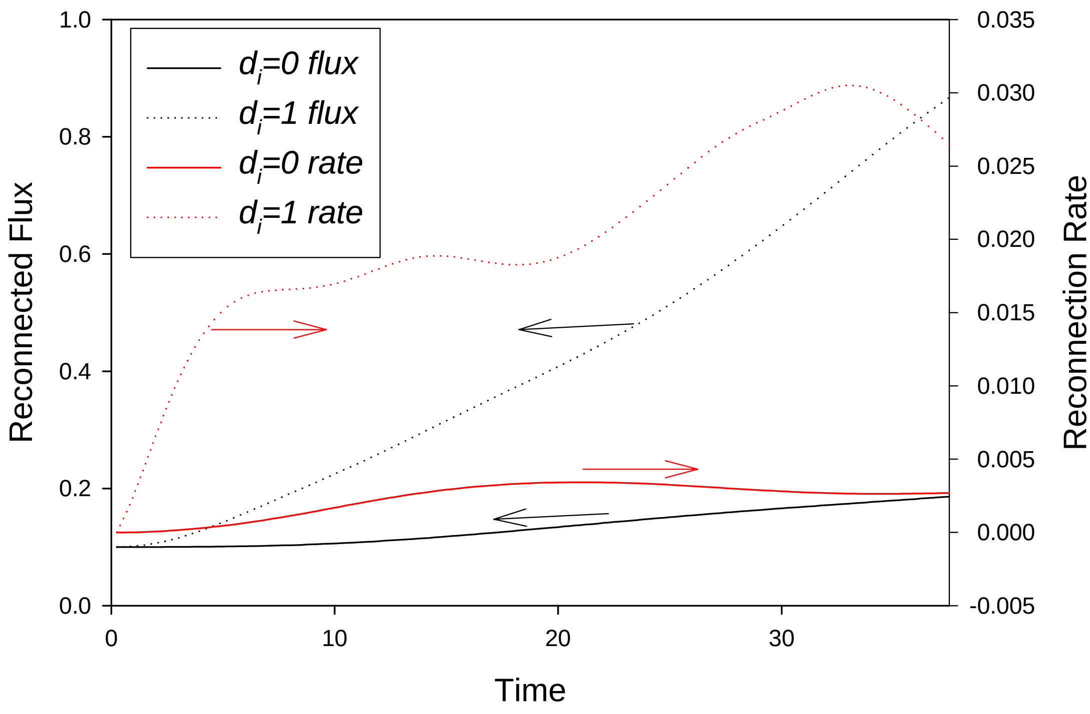

Figure 7: Comparison of the amount of reconnected flux (dark curves) and the reconnection rates (red curves) vs time for the two cases. It is seen that the Hall reconnection case with d_i*=1.0* causes reconnection to occur about 8 times faster that the resistive MHD case with d_i*=0* for these parameters.

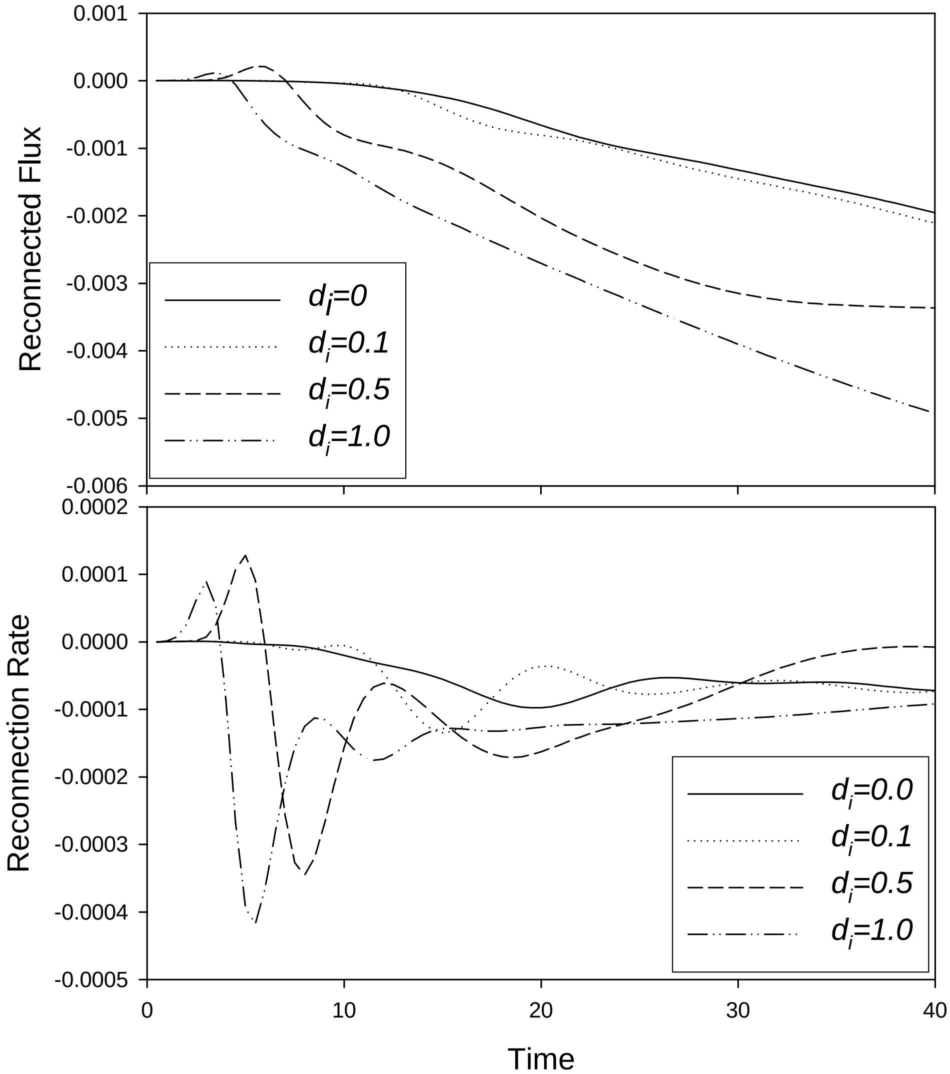

Figure 8: Reconnected flux (top) and reconnection rate (bottom) vs time for the Taylor problem for different values of the collisionless ion skin depth d_i. Other physical parameters were $\eta=\mu=10^{-4}$, $h=1$. The parameter d_i is seen to have a significant impact on the reconnection rate, especially at early time.